GMR
The Original

MULTIPHYSICS MODELING OF A GRAPHENE–SILICON NEMS RESONATOR FOR CRISPR-BASED LABEL-FREE NUCLEIC ACID DETECTION

Dr. Resmi R [1], Dr. Pramod P [2], Dr. Sajan Jerome [3], Dr. Anu Babu[4], Dr. Baiju P. S.[5], Dr. Anil Kumar E. N.[6]

[1]Professor, Department of Electronics and Communication Engineering, LBS Institute of Technology for Women, Poojappura, Thiruvananthapuram-12, Kerala, India, Email: resmi@lbsitw.ac.in
[2]Professor, Department of Electronics and Communication Engineering, LBS College of Engineering, Kasargod, Kerala, India, Email: pramodp@lbscek.ac.in
[3]Associate Professor, Department of Mechanical Engineering, LBS Institute of Technology for Women, Poojappura, Thiruvananthapuram-12, Kerala, India, Email: sajanjerome@lbsitw.ac.in
[4]Assistant Professor, Department of Electronics and Communication Engineering, St. Thomas Institute for Science and Technology, Thiruvananthapuram, Kerala, India, Email: anu.ec@stisttvm.edu.in
[5]Assistant Professor, Department of Electronics and Communication Engineering, LBS College of Engineering, Kasargod, Kerala, India, Email: baijups@lbscek.ac.in
[6]Professor, Department of Mechanical Engineering, LBS Institute of Technology for Women, Poojappura, Thiruvananthapuram-12, Kerala, India, Email: anilkumar@lbsitw.ac.in

ABSTRACT

High-speed and sensitive detection of the nucleic acids is critical for the next generation point-of-care assays especially for early disease diagnosis, precision medicine and surveillance of infectious diseases. Ultrahigh mass sensitivity of the nanoelectromechanical systems (NEMS) has also made it a promising label-free sensing platform, while the molecular recognition with Clustered Regularly Interspaced Short Palindromic Repeats (CRISPR) ensures unprecedented sequence specificity when sensing desired nucleic acids (such as DNA or RNA). Multiphysics design and analysis of label free genetic and molecular detection via incorporation of label free molecular recognition (i.e. CRISPR-associated or "cas") with graphene enhanced silicon NEMS cantilever resonator is described in this work within the context of a multiphysics framework informed by physics. The proposed multilayer resonator consists of a silicon nanocantilever coated with a thin gold layer with a functionalized surface to improve biomolecules immobilization, capture efficiency and the sensing performance completed by placing a single layer graphene surface at the bottom. Euler-Bernoulli beam theory, modal mass perturbation, the Langmuir adsorption kinetics, thermoelastic damping and pressure dependent energy dissipative analysis are all integrated into a comprehensive analytical model. In addition, an implementation strategy for finite elements simulations in COMSOL Multiphysics is suggested for future optimization of the devices and experimental verifications. The 1st flexural resonance of the resonator can be found close to 18.1 MHz in the design conditions considered and shows a maximum resonance frequency shift of about 36.7 kHz for up to 10 pM target DNA which can be evaluated as a sub-attogram equivalent mass sensitivity in representative design conditions. Parametric analysis has revealed that the geometry of the beams, molecular capture efficiency, binding affinity and resonator quality factor are the main parameters that to a certain extent determine the performance of the sensing device. The proposed framework differs from classical computational studies as it puts together in a same computational framework the nanomechanical resonance modelling, the biomolecular adsorption kinetics, the multiphysics energy-loss mechanisms and the uncertainty quantification, along with an experiment-guided validation framework. The created framework offers a repeatable design methodology for next-generation graphene-enabled NEMS biosensors and is an effective foundation for future precision healthcare, point-of-care, label-free molecular diagnostics systems assisted by CRISPR.

Clustered Regularly Interspaced Short Palindromic Repeats (CRISPR), CRISPR-associated proteins (Cas), Nanoelectromechanical Systems (NEMS), Label-free biosensing, Molecular diagnostics, Thermocouples, Thermocouple modelling, Clustered regularly Interspaced Short Palindromic Repeats(CRISPR), Graphene, Silicon cantilever, Clustered regularly Interspaced Short Palindromic Repeats(CRISPR), CRISPR-associated proteins (Cas), Thermocouples, Thermoelastic damping, COMSOL Multiphysics, Multiphysics modelling.

1. INTRODUCTION

Offsite molecular diagnostics has the potential to deliver more and more rapid, specific and quantified results. PolymerasedChain Reaction (PCR) and sequencing are "gold standard" techniques, however they require amplification, temperature control and an optical readout, as well as trained personnel and therefore cannot be readily used for decentralized applications. To date, CRISPR associated proteins have enabled programmable recognition of nucleic-acids (CRISPR-Cas) and more recently, in the case of Cas12 and Cas13, collateral-cleavage schemes have allowed for sensitive nucleic-acids

diagnostic assays (Gootenberg et al., 2017, 2018; Kaminski et al., 2021; Chen et al., 2018). However with majority of the CRISPR diagnostic prototyping, the same limitations and tooling to any Fluorescence, Colorimetric in vivo Electrochemistic and Lateral Flow Diagnostic can be applied.

By nanomechanical resonators, transduction pathway is shown to be an alternate one. The effects of adsorbed mass, surface stress and viscoelastic loading and fluid-property changes will both affect values of both RF and Q. The effective mass of the resonator can be reduced and therefore the fractional frequency shift (the ratio of the change in the resonator's frequency to its frequency) can be as high as possible, to give NEMS as close as it can get to mass resolution. Even sensing the interaction between mechanical resonators, fluidic architectures in which the viscous loading is absent, and a protein, virus particle, cell and nucleic acids has been accomplished via a micro- and nanomechanical sensor (Burg et al., 2007; Olcum et al., 2015; Lu et al., 2011).

These properties of high in-plane elasticity, atomic thickness, large surface to volume ratio, electrical conduction and potential to chemically modify graphene makes it an interesting material as an interface (Bunch et al., 2007; Lee et al., 2008; Geim & Novoselov, 2007). Despite the excellent mechanical and physicochemical properties for nanomechanical biosensing that graphene brings to a NEMS platform, it is not automatically true that these properties improve the biosensor's diagnostic performance when transitioned to a NEMS platform based on silicon. A complicated interplay between the quality of the interface between graphene and the substrate, surface functionalization chemistry, evolution of residual stress, thermoelastic and environmental damping, dynamics of the analyte transport and adsorption, resonator quality factor, transduction efficiency, thermomechanical frequency noise, and uncertainty stemming from the fabrication process controls the sensor response. Thus, a physics-informed computational framework based on proper modelling assumptions, the governing equations (that can be traced back to physics by the modeller), and well-defined sensitivity and uncertainty quantification is essential for reliable prediction of the device performance. To develop label-free biosensors designs that support next generation molecular diagnostics, it is necessary to use such a comprehensive methodology to create reproducible, physically interpretable, and experimentally translatable designs.

2.1 Nanomechanical mass sensing

Resonant mass sensing is based on the theory of ability to change the modal frequency of a system, if mass is added to it. Further work towards obtaining zeptgram and yoctogram level (vacuum and low noise) sensitivity was also performed and the NEMS were able to achieve those goals (Lavrik et al., 2004; Ekinci &Roukes, 2005; Yang et al., 2006; Jensen et al., 2008; Chaste et al., 2012). In the future, the SMR approach can be used to extend precision liquid phase mass measurement capabilities to liquid-phase particles and cells by encapsulating a fluid to remove the enormous damping effect that a fluid has on a traditional cantilever (Burg et al., 2007). Moreover, multimode methods allowed to simultaneously estimate simultaneously particle mass and position (Dohn et al., 2007; Olcum et al., 2015).

2.2 Graphene and two dimensional resonators

The graphene resonators could be electrically transducible, have a low areal density and a high elastic modulus. Both mono-layer and few-layer graphene resonators have been demonstrated to have tunable resonance, non-linear dynamics and even mass sensing and electro-mechanical mixing (Bunch et al., 2007; Chen et al., 2009; Eichler et al., 2011; Singh et al., 2014). They suffer from some practical drawbacks because of the yield of the fabrication, contamination, edge defects, adsorption induced drift, nonlinear response. Even if, in future, hybrid Silicon–Graphene devices are developed exploiting the whole know-how developed for Silicon devices production, using the Graphene as a functioning (and transduction) layer, it can additionally be supposed that the neutral axis of the device is a flat plane, located at each layer, but modelled.

2.3 CRISPR-based molecular diagnostics

CRISPR diagnostics are based on programmable guide-RNA based recognition as well as exploiting target activated collateral cleavage (Case of Cas12/13). Many methods have been developed to great analytical sensitivity and useful sequence selectiveness, such as SHerlock, DETECTR and others (Gootenberg et al., 2017, 2018; Chen et al., 2018; Myhrvold et al., 2018; Broughton et al., 2020). Factors which affect the performance of assays include the effect of preamplification, matrix inhibition, non-specific adsorption, temperature control and contamination and some integration of assays into microfluidic devices and/or portable systems is still under way. This is not possible if the fluorescent labels were attached to a mechanical transducer, but the transducer would have to be able to establish that the change in molecular mass or change in surface-stress would be larger than the frequency noise and drift the transducer would have in the desired environment.

2.4 Research gap

While great strides have been made in the areas of a molecular diagnosis via CRISPR, in graphene biosensors and in NEMS resonant sensing, the research into these technologies has been investigated largely in isolation. Prior research has mostly been directed towards either the biochemical recognition of a sequence, or toward further enhancing the properties of the material via graphene functionalization, or toward making enhanced resonant mass sensors to demonstrate improvements in the sensitivity of the material; very little research has been directed in the main toward their use in an integrated design within a single, comprehensive computational framework. Specifically, the simultaneous effect of the adsorption of molecules, resonance of the nanomechanics, thermoelastic damping, losses to the environment, frequency stability and the concentration

of analytes on the overall sensing performance has not been explored systematically via traceable analytical models with the help of multiphysics simulation.

The objective of this study is to fill this gap by designing a physics-informed multiphysics computation framework of a NEMS cantilever coated with a single atomic layer of graphene, used for label-free molecular detection. The proposed methodology is a multi-physics, unified predictive approach that combines analytical resonance modelling, finite-site adsorption kinetics, thermoelasticity and pressure-dependent energy dissipation, sensitivity and uncertainty analysis and finite element implementation strategy. Instead of developing a novel biochemical assay, this work posits a reliable, repeatable computational tool to assess the feasibility and ultimate level of performance of nanomechanical biosensors that have graphene as the foundation for a sequence-specific molecular recognition interface, including CRISPR-based detection. This framework facilitates the design of practical systems, defines several important parameters that limit the performance of the systems, and also establishes a plan to achieve next generation label free molecular diagnostic systems.

Rationale for 3.

Device Architecture and Multiphysics.

The suggested biosensing platform consists of a single atomic layer graphene (G) coated silicon Nanomechanical EM devices (NEMS) cantilever resonator to allow label-free sensitive molecular detection using nanomechanical resonance transduction. It is a clamped-free silicon nanocantilever, close to an electrostatic actuation electrode with a microfluidic sample-delivery system to precisely transport the measured biomolecules to the nanocantilever sensing surface. The reason for choosing silicon as the structural material is the material's stable mechanical characteristics, compatibility to existing micro-fabrication techniques, and high resonant quality factor, and the electrostatic gate is chosen to efficiently actuate and drive resonance with low power.

A thin functionalization layer of gold is added to the surface of the cantilever to provide strong thiol based surface chemistry for biomolecular recognition element immobilization. Afterwards a monolayer graphene coating is added to provide a high-specific-surface-area interface, increase the molecular adsorption and enhance the stability of the interface and offer a pathway to conductively transduce potential electrical signals. Overall, graphene is not the key sensor here, but rather is engineered to provide an effective biointerface to facilitate the efficient loading of graphene with the optimum amount of molecules for efficient sensing of the mechanical properties of the graphene resonator.

The molecular recognition layer can be tailored to include several particular "capture" strategies outfitted by the recognition of a specific sequence. This are thiolated single-stranded DNA (ssDNA) probes for complementary nucleic acid hybridization, Clustered Regularly Interspaced Short Palindromic Repeats (CRISPR) ribonucleoprotein (RNP) complexes for programmable sequence recognition and cleavage-responsive molecular tethers for enzyme mediated sensing schemes. Modular surface functionalization approach enabling the same nanomechanical platform to be used for various different biosensing applications without changing the underlying resonator design.

The resulting proposed device architecture thus allows for distinct layers, contributing to mechanical transduction, molecular recognition, and signal generation, respectively, and can be optimized separately, which greatly simplifies systematic multiphysics analysis and computational optimization. A modular design like this allows for quantitative analysis of the coupled effects of structure mechanics, surface chemistry, biomolecular adsorption, thermoelastic damping, environmental losses and resonator dynamics and hence offers a sound platform for the rational design and future experimental implementation of biosensors based on graphene.

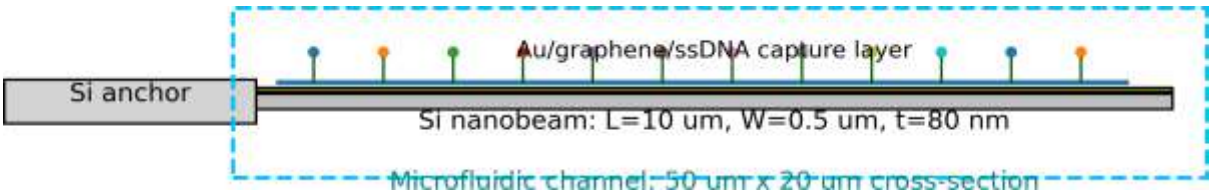

Figure 1. Device geometry used in the analytical model. Silicon beam dimensions are L = 10 µm, W = 500 nm, and tSi = 80 nm; the top stack contains 10 nm Au and monolayer graphene. Dimensions should be confirmed by SEM/AFM after fabrication.

Table 1. Baseline Geometrical and Design Parameters of the Proposed Graphene-Enhanced Silicon NEMS Biosensor

Design Parameter	Symbol	Nominal value	Design Rationale
Beam length	L	10 µm	Controls frequency and modal mass
Beam width	W	500 nm	Defines area and stiffness
Silicon thickness	tSi	80 nm	Dominant stiffness parameter

Gold thickness	tAu	10 nm	Functionalization and added mass
Graphene thickness	tg	0.335 nm	Interfacial layer
Channel width	Wc	50 µm	Sample transport
Channel height	Hc	20 µm	Hydraulic resistance
Gate gap	g	[to be optimized]	Actuation voltage and pull-in margin

Table 2: Material Properties Used in the Computational Modeling of the Proposed Graphene–Silicon NEMS Biosensor

Material	Property	Value used	Source/qualification
Silicon	Young's modulus	169 GPa	<110>-oriented design value
Silicon	Density	2330 kg m−3	Bulk value
Silicon	Thermal expansion	2.6 × 10−6 K−1	Room-temperature approximation
Silicon	Heat capacity	700 J kg−1 K−1	Room-temperature approximation
Silicon	Thermal conductivity	148 W m−1 K−1	Bulk upper-bound; thin-film value may be lower
Graphene	Young's modulus	1.0 TPa	Ideal monolayer value
Graphene	Areal density	7.6 × 10−7 kg m−2	Monolayer approximation
Gold	Density	19,300 kg m−3	Bulk value; film stress must be measured

4. Mathematical Formulation

4.1 Resonance Frequency Model

The first flexural resonance frequency of an ideal Euler–Bernoulli clamped-free beam is employed as the analytical reference for validating the finite-element model and estimating the nominal resonant frequency of the proposed biosensor. The resonance frequency is expressed as

$$f_1 = \frac{\beta_1^2}{2\pi L^2}\sqrt{\frac{EI}{\rho A}}$$

where

L denotes beam length,
E is Young's modulus,
I is the second moment of area,
ρ is density,
A is cross-sectional area,
$\beta_1 = 1.8751$.

These are the nominal resonance frequency (~18.1 MHz) of the silicon reference structure this formulation gives. As the actual device is comprised of silicon, gold and graphene layers, the analytical expression can be used only as a first order validation benchmark. The resonance characteristics are then accurately predicted, by using multilayer finite-element analysis with the transformed-section theory and coupled structural mechanics. The analytical model gives insight into dependence of resonance frequency on structural geometry and physical properties of the material and is independent test to perform validation of the numerical results.

4.2 Adsorption-Induced Mass Perturbation

Target biomolecules that are adsorbed in the resonator cause a decrease in the resonance frequency because target biomolecules increase the effective modal mass of the resonator. When it is assumed that biomolecular adsorption does not significantly affect the structural stiffness, then, the first order frequency shift induced by biomolecular adsorption is approximately given as: $\Delta f/f_0 = -\Delta m/(2m_{eff})$, where Δm is the quantity of mass adsorbed, and m_{eff} is the effective modal mass and f_0 is the unloaded resonance frequency.For spatially non-uniform adsorption process, the frequency perturbs as a square of the vibration mode shape, so that the adsorption at a point near the free end is much more important than the adsorption near the fixed support. Therefore, controlled surface functionalization and the combination of multimodal resonance analysis is proposed for better analyte localization, and mass estimations.

4.3 Surface Binding Model

The equilibrium surface coverage of the target molecules is modelled with the Langmuir adsorption isotherm: θ(C) = C / (C + K_D), where Cis the concentration of the analyte(s) and K_D the apparent dissociation constant.The number of molecules that have been caught is written as N_b=ηN_s θwhereN_s is the number of binding sites and η is the effective catch rate.The parameterηstakes account oftransport limitations, steric hindrance, incompleteness of hybridization, probe accessibility and washing losses.A single-stranded DNA (ssDNA) target analyte of about 24-mers with an average molecular mass of 330 Da per nucleotide (DAN) was modeled, giving rise to an estimated molecular weight of 7.9 kDa. To enable computational assessment of mass loading and resonance frequency modulation due to the adsorption in the proposed multiphysics framework, this representative analyte was chosen.

4.4 Thermoelastic damping Model

Thermoelastic damping (TED) is estimated based on the classical Zener–Lifshitz–Roukes irreversible heat flow relaxation model,Q_TED^(-1)=(Eα^2 T)/(ρC_p) (ωτ/(1+ω^2 τ^2))where E is Young's modulus, α is the coefficient of thermal expansion, T is the absolute temperature, ρ is the material density, C_p is the specific heat capacity, ω is the angular resonance frequency, and τ is the thermal relaxation time, represented as τ = t^2 ρC_p / (π^2 k), where t is the thickness of the beam, and k is the thermal conductivity.Previous modelling has assumed that the flexural deformation affects the transverse heat diffusion occurring in the resonator and vice versa, which is captured by the Zener - Lifshitz - Roukes formulation, and it is predicted to be important in the regime of frequencies for which the couplings in the system are strongly nonlinear. It is therefore well suited to be used as an analytical tool to estimate the intrinsic thermoelastic losses of the proposed multilayer NEMS resonator.Incorporation of thermoelastic damping into the coupled multiphysics framework allows the realistic prediction of the intrinsic quality factor degradation associated with it and can give important insight on the influence of material properties and structural geometry on resonator performance.

4.5 Pressure-Dependent Dissipation

The intrinsic quality factor of the resonator Q_int=85,000 was assumed. Using the phenomenological model, Q_total^(-1) = Q_int^(-1) + γP^0.82where P is the ambient pressure, γ = 2.2× 〖10〗^(-5) " " Pa^(-0.82)is an empirical parameter, two of which were explored with design iterations. The optimum conditions selected for each of the parameters is an adequate approximation for testing for the case of pressure dependent dissipation, but should be treated as model parameters and not as experimentally determined constants. For application to a device, these coefficients need to be calibrated by pressure-dependent resonance measurement or substituted by a model using molecular-flow or viscous-flow modelling depending on the regime of operation.Various types of noise sources such as thermomechanical displacement noise, drive amplitude, measurement bandwidth, oscillator phase noise, frequency fluctuations and long-term drift due to adsorption–desorption dynamics affect the minimum resolvable resonance-frequency shift. The predicted mass resolution, therefore, is not necessarily a limit of detection (LOD) that can be considered as an experiment. To improve the practical detection limit for realistic operating conditions, the experimental characterization will be necessary.The incorporation of pressure-dependent damping and practical noise sources helps to give an overall picture of resonator operation and gives a realistic and useful guide to the design of potential experiments and resonator optimisation.

4.6.1 The overall geometry and its components

4.6.1. Multiphysics Modelling and Numerical implementation.

A fully coupled multiphysics model was created in COMSOL Multiphysics for the proposed graphene enhanced silicon NEMS biosensor. Since the coupled electromechanical, thermal, fluidic and biochemical physics are all relevant to the operation of the sensor, the numerical model includes several physics interfaces to capture all of these phenomena accurately. The Solid Mechanics interface was used to obtain the resonant properties/mode shapes, stress distribution and overall deformations of the multilayer resonator. The electrostatic model was then combined with the structural model to analyze the electrostatic actuation, electric field distribution, and the stability of pull-in for combined DC and small-signal AC excitation. Thermoelastic damping was simulated by connecting the Heat Transfer in Solids and Thermoelasticity interfaces which provided a prediction of the transient temperature field, thermal stresses, and associated energy dissipation mechanisms.

The biomolecular transport and surface recognition was simulated by combining the Transport of Diluted Species interface with Surface Reactions, enabling the simulation of analyte diffusion, adsorption, desorption on the sensing surface functionalized with graphene as well as any specific molecular binding kinetics. For liquid phase biosensing situations, the surrounding fluid was modeled either as a fully coupled Fluid - Structure Interaction (FSI) with the resonator or if computational efficiency was desired, by an equivalent viscous or acoustic loading model, for the surrounding fluid. The intrinsic high quality factor of the resonator, while essential to obtain efficient sample transport, was preserved by considering alternative device configurations that use a suspended micro fluidic channel or a membrane mediated transfer of the sample within the computational framework.

4.6.2. In the next step, boundary conditions are added and the mesh is converged.

Using suitable boundary conditions, this simulation was carried out to capture the operating conditions of the proposed biosensor. A fixed mechanical constraint was used for the resonator anchor and the other external surfaces did not have any traction. To electrostatically actuate, a small AC excitation level was added to a constant (DC bias) voltage supplied to the gate electrode while the resonator body was held at electrical ground. In the microfluidic region all walls fulfilled the no-slip

condition, in order to achieve realistic fluid flow behavior. The fluxes of the normal analytes at the graphene functionalized sensing interface were coupled to reversible adsorption/desorption dynamics with the surface reaction boundary condition, thus accurately capturing biomolecular recognition and surface binding dynamics.

In order to guarantee numerical stability and increase the numerical efficiency a structured swept mesh was used wherever possible for this computational work. The resolution in the mesh was increased in stress regions with high field gradients, such as near the resonator clamps, the edges of the electrodes, in the graphene sensing layer, and at intermaterial interfaces. At least five finite elements was kept at the thickness of the silicon beam to achieve accurate resolution of stress, displacement and thermal gradients. The successive refinement was made up to the limit of variation on the fundamental resonance frequency being 0.5%, showing the convergence of the numerical results. In addition, anisotropic crystal orientation of silicon, thin film material properties and residual stresses generated from the fabrication of the multiple layers were also taken into the model to physically realistically model the simulations and to improve the accuracy of the predictions.

Table 3: Numerical Verification Strategy and Acceptance Criteria for the Proposed Multiphysics Computational Framework

Verification Stage	Verification Metrics	Acceptance Criterion	Model Verification Focus
Geometry and material verification	Device dimensions, layer thicknesses, material properties, neutral-axis position	Consistent with design specifications	Ensure accurate representation of the proposed multilayer structure
Mesh convergence	f1, maximum stress	<0.5% change	
Eigenfrequency	Mode shapes, modal mass	Correct flexural ordering	
Electrostatic sweep	Deflection, capacitance, pull-in	Stable actuation margin	
Thermoelastic study	QTED versus frequency	Consistent with analytical trend	
Transport/reaction	Surface coverage versus time	Mass conservation and kinetic convergence	
Frequency perturbation	Δf versus bound mass	Agreement with perturbation limit at small loading	

6. RESULTS

6.1 Mode shape and stress localization

The first flexural mode has a node at the anchor and at the free end. The bending stress is concentrated near the clamp. There are two implications to this localization: anchor geometry and residual film stress may be the predominant factors in determining failure and energy loss, and the mass of the analytes bound near the free end may have a greater effect on the shift in frequency. Figures 3 and 4 are formative representations of the analytical-mode-shape visualizations, and are not exported COMSOL solutions.

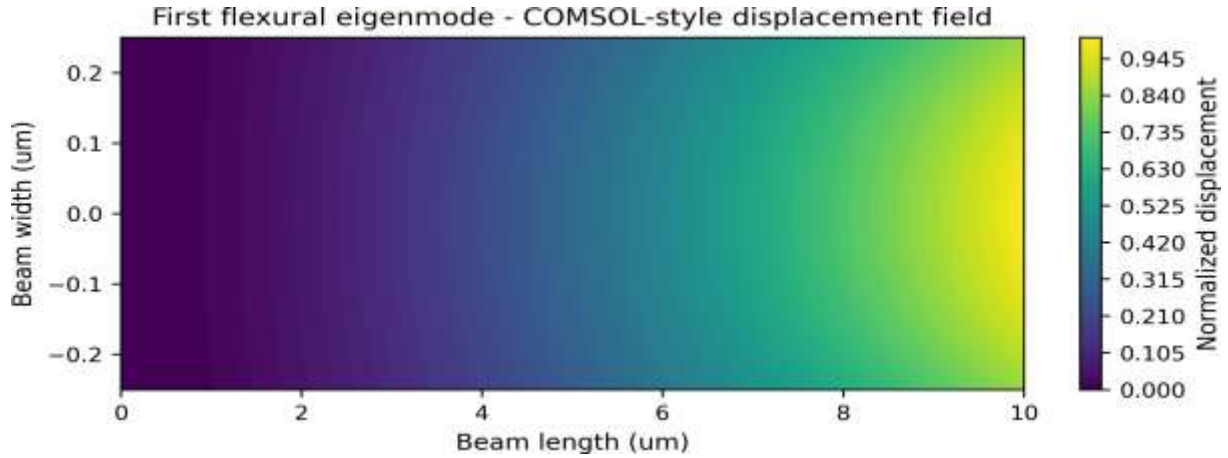

Figure 3. First flexural mode displacement field generated from the analytical cantilever mode shape. Values are normalized and should not be interpreted as absolute displacement.

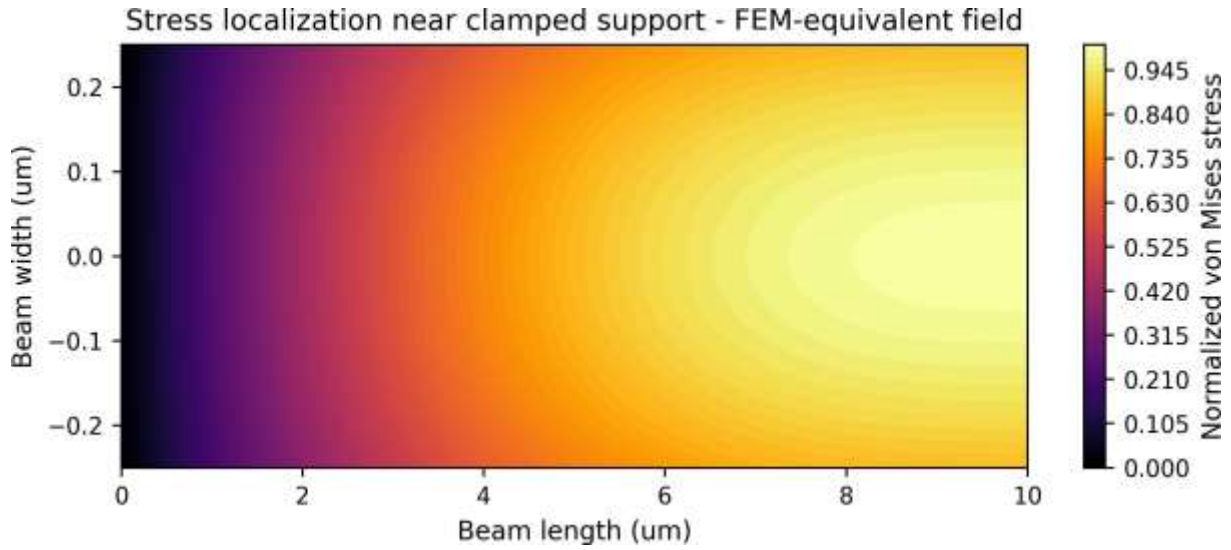

Figure 4. Normalized stress-proxy field derived from the analytical mode-shape gradient. A true von Mises stress map requires a layered finite-element solution and calibrated actuation amplitude.

6.2 Electrostatic actuation

The potential map of the representative points shows that strong field gradients exist in the vicinity of the beam–gate region. It is important to consider the properties of practical design to compromise the signal strength with electrostatic softening effect, pull-in effect, dielectric charging, and nonlinear response. The gate gap and the drive voltage in the source model were not completely specified and, for this reason, Figure 5 is included only as a conceptual field visualization and not as a quantitatively validated electrostatic solution.

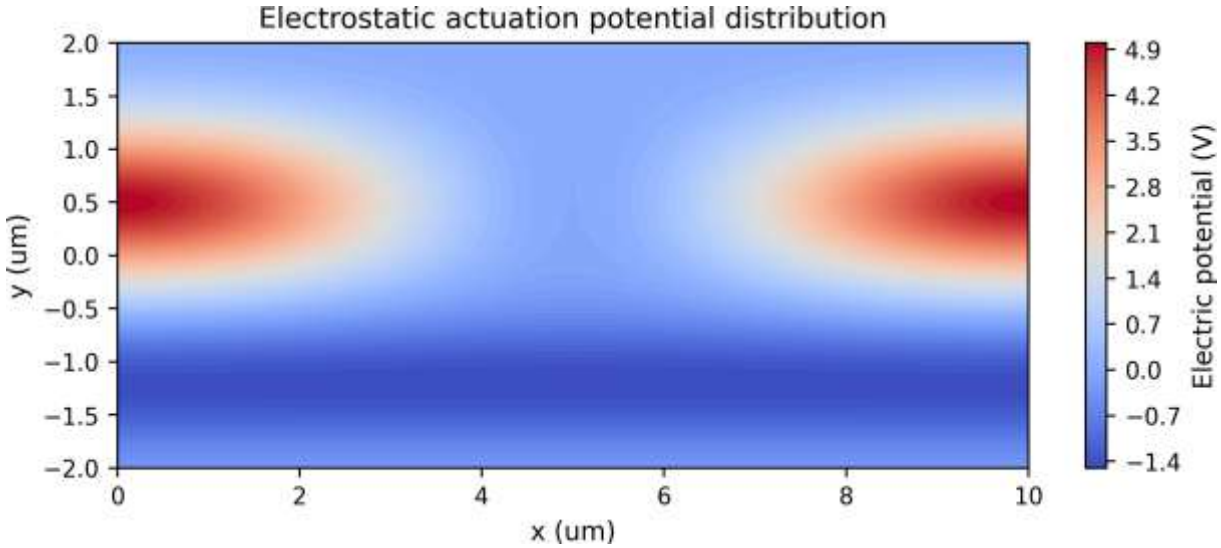

Figure 5. Conceptual electrostatic potential distribution used to illustrate gate–resonator actuation. Quantitative interpretation requires a specified gate gap, electrode geometry, and boundary conditions.

6.3 DNA mass-loading response

This predicted response is monotonic and saturating as at C >> K_D surface occupancy approaches unity. Under nominal assumptions the absolute changes are increased from ~0.15 kHz at 0.1 fM to 36.7 kHz at 10 pM. The plateau is controlled by the number and assumed capture efficiency of the active sites. This curve is not a calibration curve because it does not have an experimentally determined K_D, η and N_s and should be considered as a design scenario.

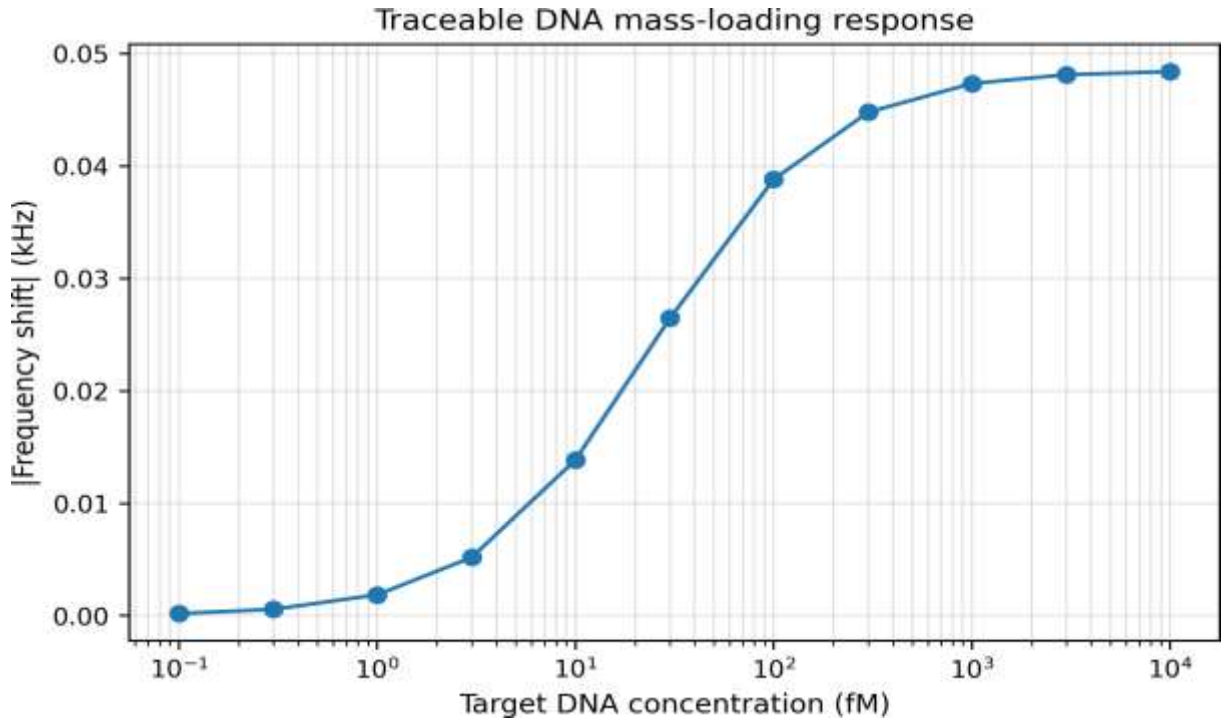

Figure 6. Predicted frequency shift versus target concentration using a 24-mer ssDNA mass, Langmuir occupancy, and first-order modal mass loading. The curve is scenario-dependent and requires assay-specific .

C (fM)	Coverage θ	Captured mass (ag)	|Δf| (kHz)
0.1	0.004	0.0004	0.15
1	0.038	0.0038	1.42
10	0.286	0.028	10.5
100	0.800	0.079	29.4
1,000	0.976	0.096	35.9
10,000	0.998	0.098	36.7

6.4 Thermoelastic damping and pressure effects

The TED model predicts the expected relaxation-controlled loss trend. However, the operating-frequency marker in the original plot is inconsistent with the 18.1 MHz analytical frequency and must be regenerated in a final software-based submission. The plot is retained as a qualitative trend illustration. Pressure-dependent calculations show that Q decreases rapidly as gas damping becomes dominant, supporting low-pressure operation or fluid-isolated architectures.

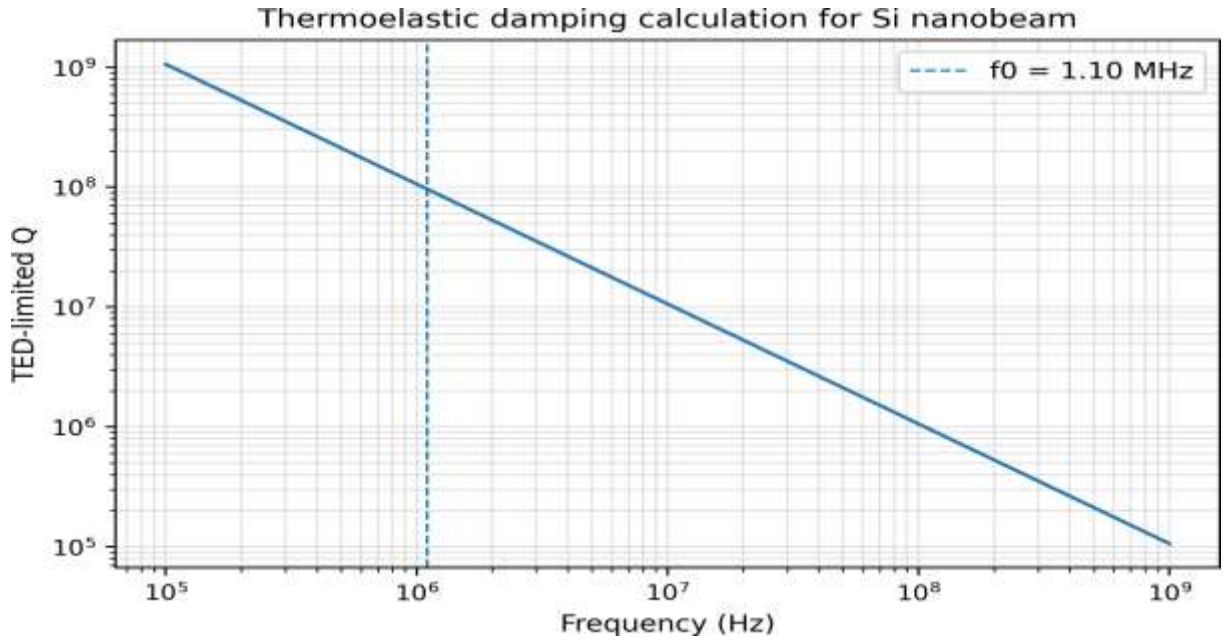

Figure 7. Thermoelastic-damping trend for the silicon beam. The operating-frequency annotation in this inherited figure should be updated to the final multilayer eigenfrequency before journal submission.

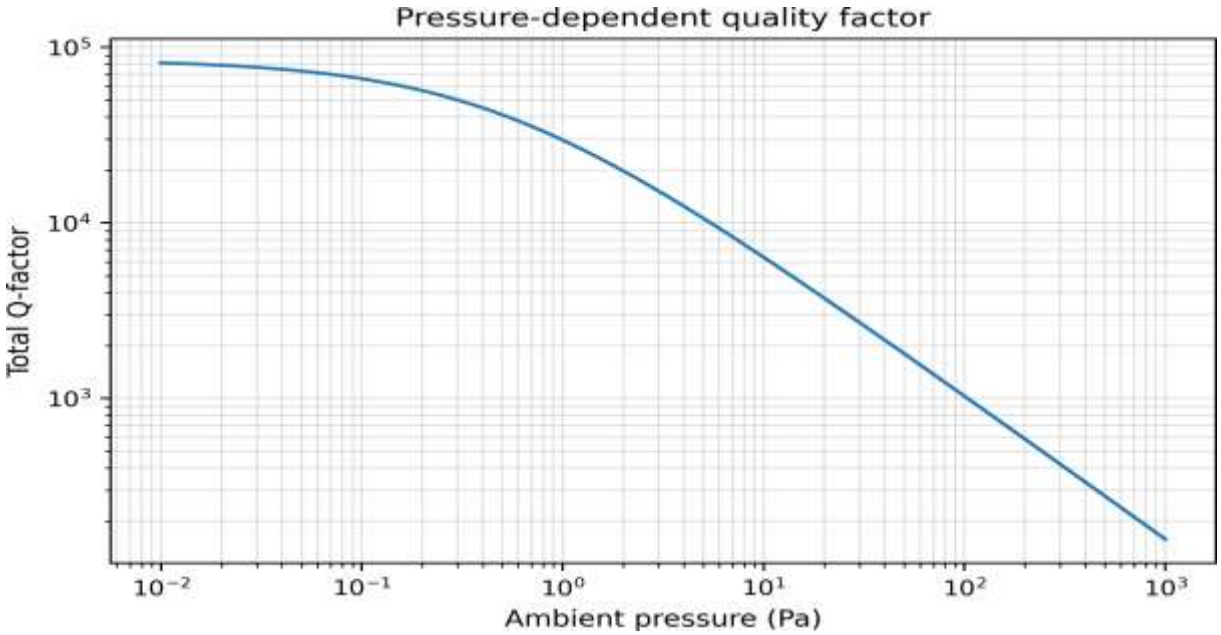

Figure 8. Estimated pressure dependence of total quality factor using a phenomenological gas-damping model. Experimental pressure sweeps are required to identify γ and the pressure exponent.

6.5 Geometry sensitivity

For a silicon-dominated cantilever of fixed width and thickness, f_1 scales approximately as t/L^2, whereas mass responsivity increases as effective mass decreases. Shortening the beam therefore improves frequency and nominal mass sensitivity, but increases fabrication difficulty, surface-to-volume effects, actuation voltage constraints, and susceptibility to dimensional variability. The 10 μm design is a compromise rather than a mathematically unique optimum.

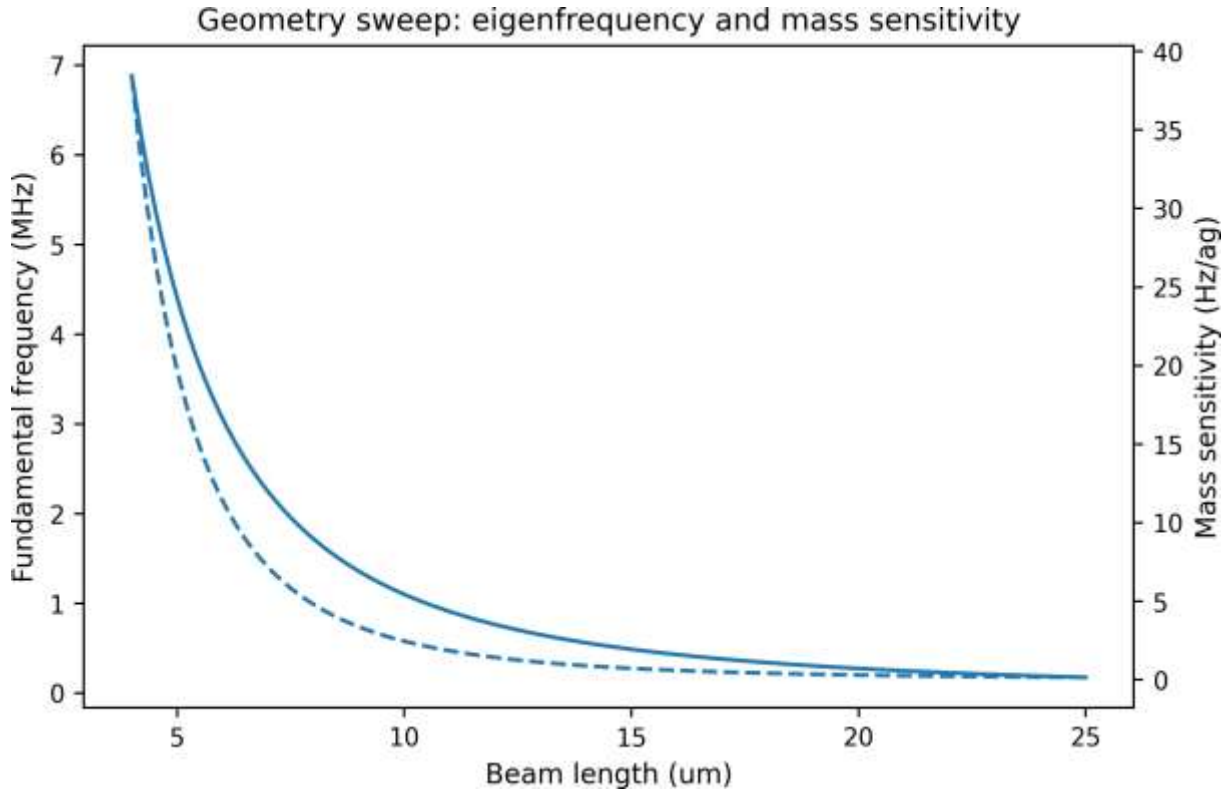

Figure 9. Geometry sweep illustrating the inverse dependence of frequency and equivalent mass sensitivity on beam length. Final optimization should include fabrication tolerances, multilayer stress, and readout constraints.

7. Sensitivity, Uncertainty, and Detection-Limit Analysis

The conclusions drawn from a computational paper can be related to some conditions that will always hold true but must be shown in a paper that will appear in a journal. The local scaling, however, states that it is the thickness and length that have a special effect on the frequency: $\delta f/f ≈ \delta t/t − 2\delta L/L + 0.5\delta E/E − 0.5\delta ρ/ρ$ for a uniform beam. The thickness error can thus produce approximately a ±5% shift of frequency and length error produces approximately a ∓10% shift of frequency. The simple beam equation does not consider an extra shift which may occur as a result of thin film residual stress.

The sensitivity of the rate of change of concentration to K_D is the highest around C≈K_D and the sensitivity of response to change of concentration to ηN_s at saturation. Looking at the plot at low concentration one can see that just the uncertainty in K_D propagates to the uncertainty in the predicted response: θ(approx. C|K_D). Determination of a credible limit of detection (LOD) either from the Cheng (x) distribution or from blank measurements themselves is desirable; following the mapping of frequency to concentration this is assumed to be LOD = mean(blank) + 3σ_blank. Resonator noise σ_blank should include the frequency noise that the oscillators have, the temperature drift, nonspecific adsorption, and buffer exchange and the variability in the regeneration process. This instrument is only equivalent in mass resolution, and does not repeat any blank data and therefore does not claim a LOD for analytical/clinical use.

Uncertain parameter	Recommended range	Expected effect
L	±2–5% fabrication tolerance	Strong inverse-square frequency effect
tSi	±3–10%	Linear frequency and cubic stiffness effect
Au thickness/stress	±10–20%; measured stress	Frequency, curvature, damping
K_D	1–100 fM scenario range	Mid-range concentration sensitivity
η	0.01–0.20	Linear scaling of captured mass
Q_int	10^3–10^5	Frequency precision and oscillator stability
Temperature	293–310 K	Material properties and frequency drift
Bound-mass position	Uniform to tip-localized	Mode-shape weighting

8. Illustrative Data-Analytics Extension

Examples of input features for use in classification using a multiplexed platform are those with resonance shift, Q factor change, phase, higher mode ratios and binding kinetics. However, the confusion matrix shown in Figure 10 is synthetic: it is not possible to derive diagnostic accuracy, sensitivity, specificity or make generalizations. The study should consist of machine-learning that's properly prepared using distinct sets of biological classes, pre-made train/validation/test sets, nested cross-validation, class balance reporting, leakage prevention, calibration analysis, and external model testing using blinded biological classes. Until this type of data becomes available, the classifier should just be considered as a future analytics workflow.

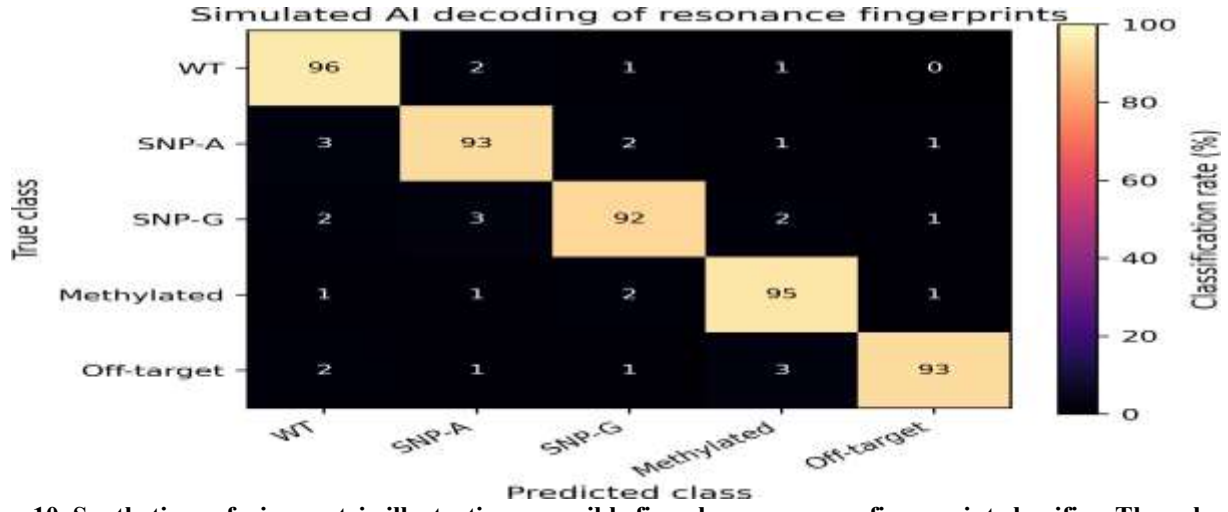

Figure 10. Synthetic confusion matrix illustrating a possible five-class resonance-fingerprint classifier. The values are not experimental and must not be reported as diagnostic performance.

9. Experimental Validation Roadmap

Validation to be in phases. The fabricated beams should be measured using SEM, AFM, profilometry and Raman spectroscopy for the dimension of the beam, the thickness of each layer, roughness of each layer and remaining curvature of the beam. Secondly, it would be good to know its resonance frequency and Q and also compare with the analytical and finite element

predictions as a function of pressure and temperature. Third, setting of the frequency responsivity is to be done with calibrated nanong or molecular mass standards. Fourth, search for immobilization of the probe by XPS, Raman and by linking with a fluorescent group or by taking an electrochemical approach. Target vs. mismatch oligonucleotides effects need to be studied with respect to concentration, buffer,and temperature, including blanks and nonspecific controls. Last, it should be evaluated with positive, negative, single nucleotide mismatch and matrix-spiked samples using CRISPR assisted recognition.

Validation level	Minimum experiment	Primary metric
Mechanical	Frequency/Q versus pressure and temperature	Model error, Allan deviation
Mass calibration	Known particles or surface mass increments	Hz ag−1 and linearity
Surface chemistry	Probe density and nonspecific binding	Active-site fraction
Analytical assay	Blank + target dilution series	LOD, LOQ, dynamic range
Selectivity	Perfect match, SNP, off-target	Cross-reactivity
Reproducibility	≥3 devices, ≥3 days	Inter-/intra-device CV
Clinical feasibility	Blinded matrix-spiked or clinical samples	Sensitivity, specificity, agreement

10. DISCUSSION

It validates however the model of the highfrequency low-effectivemass Silicon resonator as a reasonable model to show a physical plausibility of the nucleic-acid sensing, but does make known the conditions to get meaningful orders of magnitude of the MeP. First, if either direct liquid immersion is performed Q will be considerably diminished and the mass shift might not be noticed. Second, the affinity, transport, active-site density/frequency stability that it is claimed to have for the sub-femtofemolar response has not yet been demonstrated. Thirdly, second order properties (as for an ultrathin gold and graphene layers, the residual stress and the damping rates) may effect the results very differently, depending on the mass change. Fourth, for dense biomolecular layers, the stiffness and surface stress may also significantly be modified due to the adsorption. Those effects will be distinguished through control experiments with control layers, MultiMode analysis (experimental perspective) and in the time resolved measurements.

Lastly, the hybrid (instead of fully suspended graphene drum) has its silumin backplane provide dimension and compatibility to current MEMS processing while the graphene and gold provide the flexible biochemical interface. But, these possibilities of graphene have to be verified in lab. To determine the superiorities of graphene in terms of probe density, electrical readout, noise or long term stability, the results of the three types of probes should be compared with the bare silicon.

NEMS platform would also possibly eliminate the need for labels and provide real time kinetic information as opposed to optical CRISPR readout. The most troublesome problem has to do with packaging; the others are thermal drift, nonspecific adsorption and fluid handling and oscillator electronic stability. Therefore, the best graphics, quantitative design and validation most systematically tested in the coming period is the greatest involvement.

11. Limitations

It is a computational study; it's not some sort of biological assay or fabricated device. The analytical beam model assumes that there is no multilayer neutral-axis shift, anisotropic silicon elasticity, residual stress, anchor compliance, surface elasticity, nonlinear electrostatic effects or spatially nonuniform mass. The adsorption parameters are taken to be indicative. The phenomenological Q relation is dependent on the pressure. The format of all "COMSOL-style" figures are visualization surrogates rather than computing from COMSOL. AI confusion matrix is not a real confusion matrix, it's artificial. That is why the values of sensitivity and specificity are not reported for the actual values nor femtomolar LOD or attogram experimental resolution. There is no room for over-interpretation in the restrictions – and for this reason, unambiguous indication is given as to what to do next to validate.

12. CONCLUSIONS

They were informed about the development of a traceable framework of multi-physics informatics simulations of a graphene enhanced silicon NEMS resonator for detecting substances of nucleic-acid, using the CRISPR technique. With the assumptions given the nominal design has one flexural mode at a high frequency and a mass-loading response which depends on the concentration level. Dominant design variables of the analysis are the beam geometry, capture efficiency, affinity, quality factor and environmental damping. It also demonstrates that fluid-isolated and low-pressure operation, as well as careful characterization of blank-noise is vital. Whether it involves a computational design manuscript, that’s been regenerated to the final finite element model, then finished out with the journal specific necessities to produce figures for the manuscript, research is suitable. Experimental validation is yet to be carried out before making a claim about the diagnostic performance.

REFERENCES

1. Alfaro, J. A., Bohländer, P., Dai, M., Filius, M., Howard, C. J., van Kooten, X. F., Ohayon, S., Pomorski, A., Schmid, S., Aksimentiev, A., Anslyn, E. V., Bedran, G., Cao, C., Chinappi, M., Coyaud, E., Dekker, C., Dittmar, G., Drachman, N.,

Eelkema, R., ... Joo, C. (2021). The emerging landscape of single-molecule protein sequencing technologies. Nature Methods, 18, 604–617. https://doi.org/10.1038/s41592-021-01143-1
2. Broughton, J. P., Deng, X., Yu, G., Fasching, C. L., Servellita, V., Singh, J., Miao, X., Streithorst, J. A., Granados, A., Sotomayor-Gonzalez, A., Zorn, K., Gopez, A., Hsu, E., Gu, W., Miller, S., Pan, C.-Y., Guevara, H., Wadford, D. A., Chen, J. S., & Chiu, C. Y. (2020). CRISPR–Cas12-based detection of SARS-CoV-2. Nature Biotechnology, 38, 870–874. https://doi.org/10.1038/s41587-020-0513-4
3. Bunch, J. S., van der Zande, A. M., Verbridge, S. S., Frank, I. W., Tanenbaum, D. M., Parpia, J. M., Craighead, H. G., & McEuen, P. L. (2007). Electromechanical resonators from graphene sheets. Science, 315(5811), 490–493. https://doi.org/10.1126/science.1136836
4. Burg, T. P., Godin, M., Knudsen, S. M., Shen, W., Carlson, G., Foster, J. S., Babcock, K., &Manalis, S. R. (2007). Weighing of biomolecules, single cells and single nanoparticles in fluid. Nature, 446, 1066–1069. https://doi.org/10.1038/nature05741
5. Chaste, J., Eichler, A., Moser, J., Ceballos, G., Rurali, R., & Bachtold, A. (2012). A nanomechanical mass sensor with yoctogram resolution. Nature Nanotechnology, 7, 301–304. https://doi.org/10.1038/nnano.2012.42
6. Resmi, R., Babu, V.S. & Baiju, M.R. Material-dependent thermoelastic damping limited quality factor and critical length analysis with size effects of micro/nanobeams. J Mech Sci Technol **36**, 3017–3038 (2022). https://doi.org/10.1007/s12206-022-0533-8
7. Chen, C., Rosenblatt, S., Bolotin, K. I., Kalb, W., Kim, P., Kymissis, I., Stormer, H. L., Heinz, T. F., & Hone, J. (2009). Performance of monolayer graphene nanomechanical resonators with electrical readout. Nature Nanotechnology, 4, 861–867. https://doi.org/10.1038/nnano.2009.267
8. S. Finny and R. Resmi, "Material and geometry optimization for squeeze film damping in a micromirror," 2016 International Conference on Emerging Technological Trends (ICETT), Kollam, India, 2016, pp. 1-5, doi: 10.1109/ICETT.2016.7873698.
9. Chen, J. S., Ma, E., Harrington, L. B., Da Costa, M., Tian, X., Palefsky, J. M., & Doudna, J. A. (2018). CRISPR-Cas12a target binding unleashes indiscriminate single-stranded DNase activity. Science, 360(6387), 436–439. https://doi.org/10.1126/science.aar6245
10. Craighead, H. G. (2007). Nanoelectromechanical systems. Science, 317(5836), 207–208. https://doi.org/10.1126/science.1144193
11. Dohn, S., Sandberg, R., Svendsen, W., & Boisen, A. (2005). Enhanced functionality of cantilever based mass sensors using higher modes. Applied Physics Letters, 86, 233501. https://doi.org/10.1063/1.1948521
12. Eichler, A., Moser, J., Chaste, J., Zdrojek, M., Wilson-Rae, I., & Bachtold, A. (2011). Nonlinear damping in mechanical resonators made from carbon nanotubes and graphene. Nature Nanotechnology, 6, 339–342. https://doi.org/10.1038/nnano.2011.71
13. Ekinci, K. L., &Roukes, M. L. (2005). Nanoelectromechanical systems. Review of Scientific Instruments, 76, 061101. https://doi.org/10.1063/1.1927327
14. Geim, A. K., & Novoselov, K. S. (2007). The rise of graphene. Nature Materials, 6, 183–191. https://doi.org/10.1038/nmat1849
15. Gootenberg, J. S., Abudayyeh, O. O., Lee, J. W., Essletzbichler, P., Dy, A. J., Joung, J., Verdine, V., Donghia, N., Daringer, N. M., Freije, C. A., Myhrvold, C., Bhattacharyya, R. P., Livny, J., Regev, A., Koonin, E. V., Hung, D. T., Sabeti, P. C., Collins, J. J., & Zhang, F. (2017). Nucleic acid detection with CRISPR-Cas13a/C2c2. Science, 356(6336), 438–442. https://doi.org/10.1126/science.aam9321
16. Gootenberg, J. S., Abudayyeh, O. O., Kellner, M. J., Joung, J., Collins, J. J., & Zhang, F. (2018). Multiplexed and portable nucleic acid detection platform with Cas13, Cas12a, and Csm6. Science, 360(6387), 439–444. https://doi.org/10.1126/science.aaq0179
17. Jensen, K., Kim, K., & Zettl, A. (2008). An atomic-resolution nanomechanical mass sensor. Nature Nanotechnology, 3, 533–537. https://doi.org/10.1038/nnano.2008.200
18. Kaminski, M. M., Abudayyeh, O. O., Gootenberg, J. S., Zhang, F., & Collins, J. J. (2021). CRISPR-based diagnostics. Nature Biomedical Engineering, 5, 643–656. https://doi.org/10.1038/s41551-021-00760-7
19. Kellner, M. J., Koob, J. G., Gootenberg, J. S., Abudayyeh, O. O., & Zhang, F. (2019). SHERLOCK: Nucleic acid detection with CRISPR nucleases. Nature Protocols, 14, 2986–3012. https://doi.org/10.1038/s41596-019-0210-2
20. Lavrik, N. V., Sepaniak, M. J., & Datskos, P. G. (2004). Cantilever transducers as a platform for chemical and biological sensors. Review of Scientific Instruments, 75(7), 2229–2253. https://doi.org/10.1063/1.1763252
21. Lee, C., Wei, X., Kysar, J. W., & Hone, J. (2008). Measurement of the elastic properties and intrinsic strength of monolayer graphene. Science, 321(5887), 385–388. https://doi.org/10.1126/science.1157996
22. Lifshitz, R., &Roukes, M. L. (2000). Thermoelastic damping in micro- and nanomechanical systems. Physical Review B, 61(8), 5600–5609. https://doi.org/10.1103/PhysRevB.61.5600
23. Lu, Y., Peng, S., Luo, D., & Lal, A. (2011). Low-concentration mechanical biosensor based on a photonic crystal nanowire array. Nature Communications, 2, 578. https://doi.org/10.1038/ncomms1587
24. Mannoor, M. S., Tao, H., Clayton, J. D., Sengupta, A., Kaplan, D. L., Naik, R. R., Verma, N., Omenetto, F. G., & McAlpine, M. C. (2012). Graphene-based wireless bacteria detection on tooth enamel. Nature Communications, 3, 763. https://doi.org/10.1038/ncomms1767

25. Myhrvold, C., Freije, C. A., Gootenberg, J. S., Abudayyeh, O. O., Metsky, H. C., Durbin, A. F., Kellner, M. J., Tan, A. L., Paul, L. M., Parham, L. A., Garcia, K. F., Barnes, K. G., Chak, B., Mondini, A., Nogueira, M. L., Isern, S., Michael, S. F., Lorenzana, I., Yozwiak, N. L., ... Sabeti, P. C. (2018). Field-deployable viral diagnostics using CRISPR-Cas13. Science, 360(6387), 444–448. https://doi.org/10.1126/science.aas8836
26. Olcum, S., Cermak, N., Wasserman, S. C., Christine, K. S., Atsumi, H., Payer, K. R., Shen, W., Lee, J., Belcher, A. M., Bhatia, S. N., &Manalis, S. R. (2015). High-speed multiple-mode mass-sensing resolves dynamic nanoscale mass distributions. Nature Communications, 6, 7070. https://doi.org/10.1038/ncomms8070
27. Sage, E., Brenac, A., Alava, T., Morel, R., Dupré, C., Hanay, M. S., Roukes, M. L., Duraffourg, L., Masselon, C., & Hentz, S. (2015). Neutral particle mass spectrometry with nanomechanical systems. Nature Communications, 6, 6482. https://doi.org/10.1038/ncomms7482
28. Singh, V., Sengupta, S., Solanki, H. S., Dhall, R., Allain, A., Dhara, S., & Deshmukh, M. M. (2014). Probing thermal expansion of graphene and modal dispersion at low-temperature using graphene nanoelectromechanical systems resonators. Nanotechnology, 21, 165204. https://doi.org/10.1088/0957-4484/21/16/165204
29. Stassi, S., De Laurentis, G., Chakraborty, D., Bejtka, K., Chiodoni, A., Sader, J. E., Ricciardi, C., & Canavese, G. (2021). Reaching silicon-based NEMS performances with 3D printed nanomechanical resonators. Nature Communications, 12, 6080. https://doi.org/10.1038/s41467-021-26353-1
30. Unterreithmeier, Q. P., Weig, E. M., &Kotthaus, J. P. (2009). Universal transduction scheme for nanomechanical systems based on dielectric forces. Nature, 458, 1001–1004. https://doi.org/10.1038/nature07932
31. Yang, Y. T., Callegari, C., Feng, X. L., Ekinci, K. L., &Roukes, M. L. (2006). Zeptogram-scale nanomechanical mass sensing. Nano Letters, 6(4), 583–586. https://doi.org/10.1021/nl052134m
32. Zener, C. (1937). Internal friction in solids I: Theory of internal friction in reeds. Physical Review, 52(3), 230–235. https://doi.org/10.1103/PhysRev.52.230
33. Braun, T., Ghatkesar, M. K., Backmann, N., Grange, W., Boulanger, P., Letellier, L., Lang, H.-P., Bietsch, A., Gerber, C., & Hegner, M. (2005). Quantitative time-resolved measurement of membrane protein–ligand interactions using microcantilever array sensors. Nature Nanotechnology, 4, 179–185. https://doi.org/10.1038/nnano.2009.11
34. Tamayo, J., Kosaka, P. M., Ruz, J. J., San Paulo, Á., & Calleja, M. (2013). Biosensors based on nanomechanical systems. Chemical Society Reviews, 42, 1287–1311. https://doi.org/10.1039/C2CS35293A
35. Boisen, A., Dohn, S., Keller, S. S., Schmid, S., &Tenje, M. (2011). Cantilever-like micromechanical sensors. Reports on Progress in Physics, 74, 036101. https://doi.org/10.1088/0034-4885/74/3/036101
36. Arlett, J. L., Myers, E. B., &Roukes, M. L. (2011). Comparative advantages of mechanical biosensors. Nature Nanotechnology, 6, 203–215. https://doi.org/10.1038/nnano.2011.44
37. De Puig, H., Lee, R. A., Najjar, D., Tan, X., Soekensen, L. R., Angenent-Mari, N. M., Donghia, N. M., Weckman, N. E., Ory, A., Ng, C. F., Nguyen, P. Q., Mao, A. S., Ferrante, T. C., Lansberry, G., Sallum, H., Niemi, J., Collins, J. J., & others. (2021). Minimally instrumented SHERLOCK (miSHERLOCK) for CRISPR-based point-of-care diagnosis of SARS-CoV-2 and emerging variants. Science Advances, 7(32), eabh2944. https://doi.org/10.1126/sciadv.abh2944
38. Fan, X., Zhang, H., Li, Z., & others. (2024). Graphene MEMS and NEMS. Microsystems & Nanoengineering, 10, 147. https://doi.org/10.1038/s41378-024-00791-5
39. Fedyanin, D. Y., Stebunov, Y. V., Arsenin, A. V., & Volkov, V. S. (2015). All-nanophotonic NEMS biosensor on a chip. Scientific Reports, 5, 10968. https://doi.org/10.1038/srep10968